This is the accepted manuscript made available via CHORUS. The article has been published as:

Superconducting magnetoelectric effects in mesoscopic hybrid structures

Mostafa Tanhayi Ahari and Yaroslav Tserkovnyak

Phys. Rev. B **110**, L220501 — Published 5 December 2024

DOI: 10.1103/PhysRevB.110.L220501

Superconducting magnetoelectric effects in mesoscopic hybrid structures

Mostafa Tanhayi Ahari[1,2] and Yaroslav Tserkovnyak[2]

[1]*Materials Research Laboratory, The Grainger College of Engineering, University of Illinois Urbana-Champaign, Illinois 61801, USA*

[2]*Department of Physics and Astronomy & Bhaumik Institute for Theoretical Physics, University of California, Los Angeles, California 90095, USA*

In superconductors that lack inversion symmetry, a supercurrent flow can lead to nondissipative magnetoelectric effects. We offer a straightforward formalism to obtain a supercurrent-induced magnetization in superconductors with broken inversion symmetry, which may have orbital, layer, sublattice, or valley degrees of freedom—multiband noncentrosymmetric superconductors. The nondissipative magnetoelectric effect may find applications in fabricating quantum computation platforms or efficient superconducting spintronic devices. We explore how the current-induced magnetization can be employed to create and manipulate Majorana zero modes in a simple hybrid structure.

Introduction.—Hybrid structures involving magnetic materials and normal metals are one of the building blocks of spintronic devices. Motivated by mitigating dissipation and enhancing device performance, combining superconductivity with spintronics has led to interesting equilibrium and nonequilibrium phenomena that fuel interest in superconducting spintronics [1]. The injection of a spin-polarized (super)current into the superconductor, whose transport may be facilitated by an unconventional superconducting order, such as a triplet pairing, has been of central interest. In this Letter, we primarily focus on the effect of the supercurrent-induced magnetization on an adjacent material in a hybrid structure with an emphasis on potential utility in superconducting spintronics and quantum computation devices.

In multiband superconductors, where electrons have multiple degrees of freedom, such as orbital, layer, sublattice, or valley, a supercurrent flow may lead to a sizeable induced magnetization. The source of the induced magnetization is spin polarization [2] and/or orbital magnetic moments [3], where the former is due to spin-orbit coupling (SOC) and the latter is related to a Berry curvature of the Bloch electronic bands in these materials. Importantly, the supercurrent-induced orbital magnetization can be orders of magnitude greater than that due to the spin [4]. Due to the increasing accessibility of multiband superconductors with strong SOC, such as TMDs (transition metal dichalcogenides) [5], or large orbital moments, such as twisted bilayer graphene [6–8], the supercurrent-induced magnetoelectric effects may play a more functional role in mesoscopic hybrid structures, particularly in enhancing the efficiency of magnetic memory manipulations [9].

In this Letter, we offer a simple formulation of superconducting magnetoelectric effects for multiband superconductors in the static regime, encompassing both orbital and spin magnetization contributions. The superconducting magnetoelectric effect has been studied in Ref. [8], where the evolution of the magnetoelectric effect across the superconductor-normal metal phase transition is discussed. As we show, our results do not match Ref. [8] (in the DC limit) and reveal a greater sensitivity to the characteristics of the pairing gap function. Therefore, we suggest that our approach more accurately accounts for the influence of anisotropic pairing gaps. Importantly, the magnetization induced by supercurrents in our study may provide additional means to probe the unconventional superconducting pair potentials. Furthermore, we provide an expression for supercurrent flow in multiband superconductors that agrees with earlier results, such as those in Refs. [10–12], establishing connections between supercurrent density, Fermi surface parameters, and the superconducting energy gap. Additionally, we highlight the reciprocal nature of this phenomenon: Coupling to a dynamic magnetization, such as that of an adjacent magnet, or an applied magnetic field can induce supercurrent. Conversely, supercurrent-induced magnetization can exert torque on the adjacent magnet [see Fig. 1].

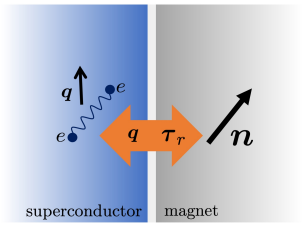


FIG. 1. Schematic of a superconductor-magnet hybrid structure. When the inversion symmetry in the superconductor is broken, a uniform supercurrent with Cooper momentum $2\boldsymbol{q}$ may induce magnetization $\boldsymbol{M}(\boldsymbol{q})$, which can exert a torque $\boldsymbol{\tau}_r \sim \boldsymbol{M}(\boldsymbol{q}) \times \boldsymbol{n}$ on the adjacent magnet. Reciprocally, coupling to the magnetization $\boldsymbol{n}$ can induce a supercurrent $\boldsymbol{j}_s$, e.g., for a superconductor with an out-of-plane polar axis $\hat{z}$, one gets $\boldsymbol{j}_s \propto \hat{z} \times \boldsymbol{n}$.

When a superconductor is in contact with a non-superconducting material, a weak superconductivity is

induced in the normal material over mesoscopic distances (superconducting proximity effect) [13]. We will show that the topological character of the induced superconductivity in the normal material can be controlled by the magnetoelectric effect in the "parent" superconductor. The physics here is analogous to the induced topological phase in a quantum wire discussed in Ref. [14], where zero-energy Majorana bound states are formed in the topological phase. However, here we propose a setup in which the Majorana fermions are electrically created and manipulated via the magnetoelectric effect, without the need for an external magnetic field. In particular, we propose a simple supercurrent protocol that realizes a braiding operation for the Majorana zero modes in a trijunction formed by the wires. Our setup can be relevant for fabricating a platform for quantum computation in a web of nanowires [15–17].

Magnetoelectric effect in multiband superconductors.—From the viewpoint of symmetry, a linear current-induced magnetization can occur if inversion symmetry is broken [18, 19] (a noncentrosymmetric material). As a result, we consider a superconductor with broken inversion symmetry described by a time-reversal symmetric normal state Hamiltonian $H_0(\boldsymbol{p})$. We assume that close to the Fermi surface, the Bloch band Kramers' splitting due to the broken symmetry is much larger than the superconducting gap, as is often a realistic limit for the multiband superconductors [20, 21]. This assumption justifies a semiclassical treatment of small perturbations (relative to the band splitting), under which the electron dynamics would be confined within the individual Bloch bands. Moreover, in the superconducting state, Cooper pairs are formed by time-reversal electron partners belonging to the same Bloch band with opposite momentum $|u_{\nu,\boldsymbol{p}}\rangle$ and $|u_{\nu,-\boldsymbol{p}}\rangle$ [22], where ν is the band index. It has been shown that the resultant "intraband" Cooper pairing is the energetically favorable (stable) superconducting state [23, 24]. As a consequence of projecting physical quantities onto a single band, we focus on the intraband effects, with interband contributions related to quantum metric effects being overlooked [11, 12, 25–27] (see the Discussion for further details). The Bogoliubov-de Gennes Hamiltonian written in the Bloch band basis reads

$$\hat{H}(\boldsymbol{p}) = \begin{pmatrix} \xi(\boldsymbol{p}) & \Delta(\boldsymbol{p}) \\ \Delta^*(\boldsymbol{p}) & -\xi(\boldsymbol{p}) \end{pmatrix}, \tag{1}$$

where $\xi(\boldsymbol{p}) = \xi(-\boldsymbol{p})$ is a diagonal matrix whose entries are the Bloch band energies $\xi_\nu(\boldsymbol{p})$ (measured from chemical potential), which are obtained by a unitary transformation $U_{\boldsymbol{p}}\, H_0(\boldsymbol{p})\, U_{\boldsymbol{p}}^\dagger = \xi(\boldsymbol{p})$. The pairing gap function $\Delta(\boldsymbol{p}) = U_{\boldsymbol{p}}\, \Delta_0(\boldsymbol{p}) U_{-\boldsymbol{p}}^{\mathrm{T}}$ is a diagonal matrix with elements $\Delta_\nu(\boldsymbol{p})$, where $\Delta_0(\boldsymbol{p})$ is the usual pairing function written in the space of the electronic degrees of freedom such as spin and valley [28]. Finally, the quasiparticle energy for band ν is given by $E_\nu = \sqrt{\xi_\nu^2 + |\Delta_\nu|^2}$.

Under a uniform supercurrent flow, quasiparticle energies get shifted (Doppler shift [29, 30]) as $E_\nu + \boldsymbol{q}\cdot\boldsymbol{v}_\nu$, where $\boldsymbol{v}_\nu = \nabla_{\boldsymbol{p}}\xi_\nu(\boldsymbol{p})$, and $2\boldsymbol{q}$ is the Cooper pair momentum ($\boldsymbol{q}/m_e$ is usually called the superfluid velocity, where m_e is the electron mass). It can be checked [28] that the total supercurrent and supercurrent-induced magnetization can be written as $\boldsymbol{j}_s = \mathbb{T}\cdot\boldsymbol{q}$ and $\boldsymbol{M} = \mathbb{Q}\cdot\boldsymbol{q}$, respectively, where

$$\mathbb{T}_{ij} = \int d\boldsymbol{\tau} \sum_\nu \Big(\frac{\partial f_\nu}{\partial E_\nu} v_{\nu,j} - \frac{\partial n_\nu}{\partial p_j} \Big) e v_{\nu,i}, \tag{2a}$$

$$\mathbb{Q}_{ij} = \int d\boldsymbol{\tau} \sum_\nu \Big(\frac{\partial f_\nu}{\partial E_\nu} v_{\nu,j} - \frac{\partial n_\nu}{\partial p_j} \Big) M_{\nu,i}. \tag{2b}$$

Here, $f_\nu \equiv f(E_\nu)$ is the Fermi-Dirac distribution function which determines the quasiparticle occupancy, $n_\nu = \frac{1}{2}\Big(1 - \frac{\xi_\nu}{E_\nu}(1-2f_\nu)\Big)$ is the occupancy of the electronic single-particle state at band ν with momentum $\boldsymbol{p}$ in the superconducting state [10, 31], and $d\boldsymbol{\tau} = d^dp/(2\pi\hbar)^d$ with d being the dimension of the system. $\boldsymbol{M}_\nu(\boldsymbol{p})$ is the total magnetization pertaining to Bloch band ν that can be decomposed into spin and orbital [19] components, $\boldsymbol{M}_\nu(\boldsymbol{p}) = \boldsymbol{s}_\nu(\boldsymbol{p}) + \boldsymbol{m}_\nu(\boldsymbol{p})$, where

$$\boldsymbol{s}_\nu(\boldsymbol{p}) = \langle u_{\nu,\boldsymbol{p}} | g\mu_{\mathrm{B}} \frac{\boldsymbol{\sigma}}{2} | u_{\nu,\boldsymbol{p}} \rangle \tag{3}$$

is the spin magnetic moment, and $\boldsymbol{m}_\nu(\boldsymbol{p})$ is the orbital magnetic moment [32, 33] for a 3D crystal

$$\boldsymbol{m}_\nu(\boldsymbol{p}) = \frac{e\hbar}{2} \mathrm{Im} \big\langle \nabla_{\boldsymbol{p}} u_{\nu,\boldsymbol{p}} \big| \times \big[H_0(\boldsymbol{p}) - \xi_\nu(\boldsymbol{p}) \big] \big| \nabla_{\boldsymbol{p}} u_{\nu,\boldsymbol{p}} \big\rangle. \tag{4}$$

A nonzero orbital magnetic moment is an intrinsic property of the band that can roughly be interpreted as a self-rotation of the electron wave function around its center of mass [32], which could indicate a nonzero Berry curvature $\boldsymbol{\Omega}_{\nu,\boldsymbol{p}} = i\hbar^2 \langle \nabla_{\boldsymbol{p}} u_{\nu,\boldsymbol{p}} | \times | \nabla_{\boldsymbol{p}} u_{\nu,\boldsymbol{p}} \rangle$ in the band structure.

The terms proportional to $\partial n_\nu/\partial p_j$ in Eqs. (2) differ from those obtained in Ref. [8] (in the DC limit), wherein the normal state occupancy of the single-particle state at band ν, denoted as $f(\xi_\nu)$, is employed instead of n_ν [34]. However, Eq. (2a) concurs with the conventional (intraband) superfluid density as established in prior studies [10–12], where the terms proportional to $\partial f_\nu/\partial E_\nu$ and $\partial n_\nu/\partial p_j$ are identified, respectively, as the paramagnetic and diamagnetic contributions to the supercurrent [30]. This alignment offers reassurance regarding the validity of Eq. (2b) in capturing the intraband current-induced magnetization. The dependence of n_ν on the superconducting pair potential enhances the sensitivity of our results to nonuniform (in momentum space) gap functions. Given the growing discovery of superconductivity in layered Van der Waals materials with anisotropic pairing gap functions, our findings are particularly relevant for understanding how such unconventional gaps influence the magnetoelectric response.

Application to two and four-band models.—Let us first consider a two-band system described by a normal state Hamiltonian $H_0(\boldsymbol{p}) = \xi_{\boldsymbol{p}}\sigma_0 + \mathbf{g}_{\boldsymbol{p}}\cdot\boldsymbol{\sigma}$, where $\boldsymbol{\sigma}$ is the vector of Pauli matrices acting on the spin basis, and σ_0 is a 2×2 identity matrix. As a result of broken inversion symmetry, $\mathbf{g}_{\boldsymbol{p}} = -\mathbf{g}_{-\boldsymbol{p}}$, the spin degeneracy of electrons is lifted suggesting a two-band description of the Fermi surface $\xi_\nu(\boldsymbol{p}) = \xi_{\boldsymbol{p}} + \nu|\mathbf{g}_{\boldsymbol{p}}|$, with $\nu = \pm1$ labeling the bands. Finally, it can be checked that the spin magnetic moment of band ν is given by $\boldsymbol{s}_\nu(\boldsymbol{p}) = \langle u_{\nu,\boldsymbol{p}}|g\mu_{\rm B}\frac{\boldsymbol{\sigma}}{2}|u_{\nu,\boldsymbol{p}}\rangle = \frac{\nu}{2}g\mu_{\rm B}\hat{\mathbf{g}}_{\boldsymbol{p}}$.

$H_0(\boldsymbol{p})$ can also describe a minimal model for novel quantum systems such as Weyl semimetals, in which $\boldsymbol{\sigma}$ acts on orbital space (valence and conduction orbitals mixed with spin), e.g., see [35, 36]. In this case, the orbital magnetic moment is given by $m_{\nu,i}(\boldsymbol{p}) = -\frac{\hbar e}{2}\varepsilon_{ijl}\frac{1}{|\mathbf{g}_{\boldsymbol{p}}|^2}\mathbf{g}_{\boldsymbol{p}}\cdot(\partial_{p_j}\mathbf{g}_{\boldsymbol{p}}\times\partial_{p_l}\mathbf{g}_{\boldsymbol{p}})$, where ε_{ijl} is the rank-3 Levi-Civita tensor [19].

Next, we consider a bilayer system with a spin-independent coupling between layers,

$$H_0 = \begin{pmatrix} H_1 & V \\ V & H_2 \end{pmatrix}, \tag{5}$$

where H_i is the Hamiltonian of layer $i = 1, 2$, and $V = \lambda\sigma_0$ with λ being the interlayer interaction [37]. As illustrative examples, we consider each layer to be described by a 2D Rashba or Dresselhaus Hamiltonian $H_i = (\frac{p^2}{2m_e} - \mu)\sigma_0 + \mathbf{g}^i_{\boldsymbol{p}}\cdot\boldsymbol{\sigma}$, where $\mathbf{g}^i_{\boldsymbol{p}} = \alpha_i(p_y, -p_x)$ and $\mathbf{g}^i_{\boldsymbol{p}} = \alpha_i(p_x, -p_y)$ for the Rashba and Dresselhaus systems, respectively. The band dispersion relation is given by

$$\xi_\nu(\boldsymbol{p}) = \frac{p^2}{2m_e} - \mu + a_1|\mathbf{g}^+_{\boldsymbol{p}}| + a_2\sqrt{|\mathbf{g}^-_{\boldsymbol{p}}|^2 + \lambda^2}, \tag{6}$$

where $\mathbf{g}^\pm_{\boldsymbol{p}} = (\mathbf{g}^1_{\boldsymbol{p}} \pm \mathbf{g}^2_{\boldsymbol{p}})/2$ and $a_1, a_2 = \pm1$. Here we identify indices $(a_1, a_2) = (1,1), (-1,1), (1,-1)$, and $(-1,-1)$, with $\nu = 1, 2, 3$ and 4, respectively. For the Rashba system, Fig. 2(a) shows the normal state energy spectrum. Eqs. (3) and (4) can now be used to evaluate the spin and orbital magnetization in the band basis. For the Rashba system [37], we get

$$\boldsymbol{s}_\nu = \frac{a_1}{2}g\mu_{\rm B}\hat{\mathbf{g}}_{\rm R}, \tag{7a}$$

$$\boldsymbol{m}_\nu(\boldsymbol{p}) = \mathrm{sign}[\alpha_+]\frac{a_1}{4}\frac{et\lambda^2\alpha_-}{|\mathbf{g}^-_{\boldsymbol{p}}|^2 + \lambda^2}\hat{\mathbf{g}}_{\rm R}, \tag{7b}$$

where $\hat{\mathbf{g}}_{\rm R} = (p_y, -p_x)/p$, $\alpha_\pm = \alpha_1 \pm \alpha_2$, and t is the distance between the layers [39]. We note that the magnitude of the spin magnetic moment is solely determined by the g-factor, while the orbital moment is influenced by multiple parameters, offering greater tunability. Fig. 2(b) shows the the orbital magnetization in the y-direction vs momentum p_x for bands $\nu = 3$ and 4. Note that $\boldsymbol{m}_\nu(\boldsymbol{p})$ for bands $\nu = 1$ and 2 is identical to bands $\nu = 3$ and 4,

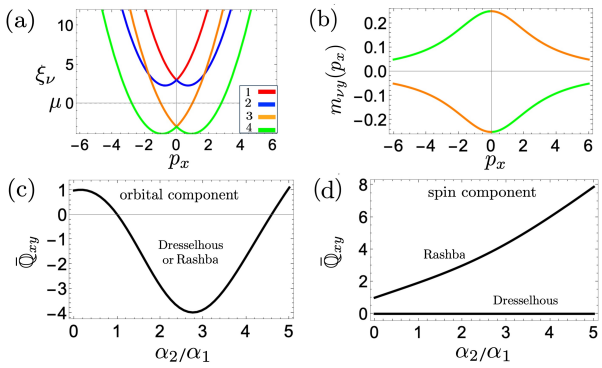


FIG. 2. (a) Schematic of band dispersion in the normal state. The inset shows $\nu = 1, 2, 3$ and 4 bands, which represent indices $(a_1, a_2) = (1,1), (-1,1), (1,-1)$, and $(-1,-1)$, respectively. (b) The orbital magnetic moment in the y-direction vs p_x for bands $\nu = 3, 4$. In this plot, we set $\alpha_1 = e = t = 1$ and $\alpha_2 = 3$. (c) Orbital component of $\bar{\mathbb{Q}}_{xy} \equiv \mathbb{Q}_{xy}/\mathbb{Q}_{xy}|_{\alpha_2=0}$ vs the strength of SOC ($\alpha_1 = 1$). The Rashba and Dresselhaus SOC have the same contribution to the orbital magnetization. (d) Spin component of $\bar{\mathbb{Q}}_{xy}$ vs strength of SOC ($\alpha_1 = 1$). For the Dresselhaus system, the spin component is zero for all α_2 values. As a result, to avoid confusion about renormalized $\mathbb{Q}_{xy}$, the plot shows $\mathbb{Q}_{xy} = 0$. Here, we use a temperature-dependent gap function $\Delta(T) = \Delta_0(1 - T/T_c)^2(1 + 2.2T/T_c)$ [38], and parameters are set to $m_e = 0.4, \mu = 0, \lambda = 3, \Delta_0 = 0.5, T = 0.1T_c$.

respectively. For the Dresselhaus system, we get

$$\boldsymbol{s}_\nu = \frac{a_1}{2}g\mu_{\rm B}\hat{\mathbf{g}}_{\rm D}, \tag{8a}$$

$$\boldsymbol{m}_\nu(\boldsymbol{p}) = \mathrm{sign}[\alpha_+]\frac{a_1}{4}\frac{et\lambda^2\alpha_-}{|\mathbf{g}^-_{\boldsymbol{p}}|^2 + \lambda^2}\hat{\mathbf{g}}_{\rm R}, \tag{8b}$$

where $\hat{\mathbf{g}}_{\rm D} = (p_x, -p_y)/p$. It is interesting to note that, unlike the Rashba SOC, in the Dresselhaus SOC, the magnetic moment perpendicular to the current direction is only due to the orbital one. Moreover, the orbital moment has the same direction for both systems, as it can be seen from Eqs. (8b) and (7b). In both systems, a non-zero orbital magnetic moment arises from the fact that the electron state in a band can be a superposition of two layers with different Fermi velocities. Consequently, a similar Fermi pocket shift due to Rashba or Dresselhaus SOC can lead to an equivalent orbital magnetic moment. To obtain the current-induced magnetization, we consider the induced magnetization in the y-direction by a current in the x-direction. Fig. 2(c) and (d) show the orbital and spin component of $\bar{\mathbb{Q}}_{xy} \equiv \mathbb{Q}_{xy}/\mathbb{Q}_{xy}|_{\alpha_2=0}$ vs relative strength of SOC.

Topological superconductivity manipulated by the magnetoelectric effect.—Consider a semiconductor wire with Rashba spin-orbit coupling (such as electron-doped InAs [40]), where proximity to a superconducting substrate induces superconducting pairing. In the presence of an external Zeeman field, the spin degeneracy of electronic bands in the wire is broken, potentially leading

to a transition to a topological phase, as discussed in Ref. [41]. This transition corresponds to symmetry class D in the Altland-Zirnbauer classification, characterized by a nontrivial Z_2 topological number and zero-energy Majorana edge modes.

Additionally, as outlined in Ref. [14], a supercurrent flowing in the substrate superconductor can induce such a transition in the wire. Interestingly, the supercurrent can lower the critical Zeeman field required for the topological phase transition. This suggests the possibility of a topological phase transition solely driven by the supercurrent, without the need for an external Zeeman field, which breaks time-reversal symmetry. Various model superconductors with diverse spin-orbit couplings have been examined in Ref. [42], showing that a finite supercurrent alone can trigger a topological phase transition. However, in simple s-wave superconductors, a relatively high supercurrent density is necessary for this transition, resulting in the quasiparticle spectrum intersecting the zero-energy level and burying the Majorana states within the bulk continuum.

We propose an alternative approach to topological superconductivity induced and manipulated by supercurrent-induced magnetization. We consider a semiconducting wire with Rashba SOC placed on top of a superconducting TMD, as shown in Fig. 3(a). Quasi-2D superconducting TMDs with C_1, C_2, C_{1v}, or C_{2v} point group symmetry possess an in-plane polar axis, which allows an in-plane supercurrent to induce an out-of-plane magnetization $\boldsymbol{M}(\boldsymbol{q})$ [18]. The substrate superconductor affects the wire band structure in two ways: an effective Zeeman field on the wire $\sim \boldsymbol{M}(\boldsymbol{q})$ and proximity induced superconductivity with a pairing $\Delta(\boldsymbol{q}) = \Delta_0\, e^{i2q_{||}r_W/\hbar}$, where $q_{||}$ is the Cooper pair momentum component parallel to the wire and r_W is the position vector along the wire, see Fig. 3(a). The extra phase factor leads to a Doppler shift in the quasiparticle spectrum of the wire. For simplicity focusing on $\mu = 0$, as discussed in Ref. [14], the boundary between topologically trivial and nontrivial (gapped) phases in a 1D superconductor is when the Zeeman energy in the wire is $E_Z = \sqrt{\Delta_0^2 - \alpha_W^2 q_{||}^2} > \Delta_0^2/4E_{SOC}$, where $E_{SOC} = m_e\alpha_W^2/2 \gg \Delta_0$ is the SOC energy scale in the wire and α_W determines the Rashba SOC in the wire. The lower limit for the Zeeman energy, $\Delta_0^2/4E_{SOC}$, ensures that the phase transition takes place between two trivial and nontrivial gapped phases, which is essential in realizing the isolated Majorana zero modes. Specifically, considering $\Delta_0 = 0.1$ meV and $E_{SOC} = 0.1$ eV, the induced Zeeman energy in the wire must be $E_Z > 10^{-4}$ meV. As a result, the topological phase transition may occur at some momentum, denoted by $|\boldsymbol{q}| = q_T$. To enhance the effective Zeeman field on the wire and to maintain q_T below the critical depairing momentum in the substrate superconductor, a semiconductor wire with a large g-factor can be employed [43].

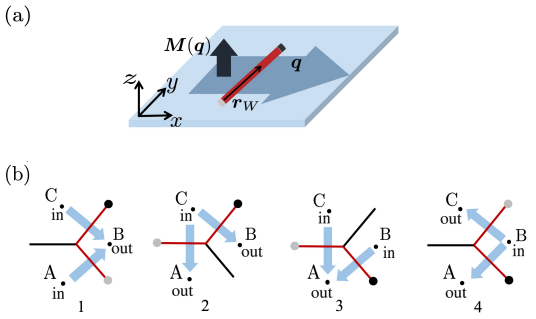


FIG. 3. (a) Schematic of a quantum wire with SOC on a superconductor. The supercurrent flow characterized by $\boldsymbol{q}$ induces a Zeeman field on the wire leading to a topological phase transition. The nontrivial phase has two Majorana modes that appear on both ends of the wire (shown by gray shades). (b) Adiabatic exchange of two Majorana bound states. The segments in red are topologically nontrivial ($q > q_T$), where the localized Majorana modes are sketched as the (light and dark shade) grey circles at the ends of the wires. The supercurrent direction and magnitude can be controlled by electrodes connected to the superconductor at points A, B, and C. Starting from a supercurrent between A-B and C-B (configuration 1), we can decrease the A-B current and simultaneously increase C-A current to transition to configuration 2 adiabatically. Now, decreasing C-B and increasing B-A currents results in configuration 3. Similarly, by decreasing C-A and increasing B-C, we return to configuration 1 with the reversed current directions, in which the Majorana modes are exchanged. Repeating the same steps resets the currents and leads to a double exchange (braiding) of Majorana modes.

The supercurrent-induced topological phase may enable the implementation of quantum computation operations using Majorana modes. To see this, consider a trijunction fabricated from the wires on the substrate superconductor [28]. When a finite supercurrent $|\boldsymbol{q}| > q_T$ is crossing a branch of wire in the trijunction, the wire is in the nontrivial phase. Consequently, as sketched in Fig. 3(b), an adiabatically slow switching of the supercurrent flow between points A, B, and C leads to the exchange of the Majorana zero modes. The supercurrent switching steps here leads to a similar adiabatic exchange of Majorana fermions first proposed in Ref. [15], where tunable local gate voltages were employed to perform an exchange operation. However, here we propose a supercurrent-induced exchange operation. We note that a double exchange (braiding) operation could realize a σ_z gate [17]. If the two Majorana fermions comprising a qubit share no quasiparticle (even electron parity) the braiding leaves the qubit unchanged. However, if the qubit has an odd electron parity, the braiding gives a minus sign.

Discussion.—For a Rashba system with SOC strength of $\alpha_1 = 2\alpha_2 = 5 \times 10^4$ m/s [44], the estimated spin and orbital magnetizations are $10^{-2}\xi^{-1}\ \mu_B/\text{nm}^2$ and $10^{-5}\xi^{-1}\ \mu_B/\text{nm}^2$, respectively, where ξ is the supercon-

ducting coherence length in nanometers. For a superconductor with $\xi = 90$ nm, the corresponding magnetizations would be $10^{-4}\mu_B/\text{nm}^2$ for spin and $10^{-7}\mu_B/\text{nm}^2$ for orbital magnetization. We note that measuring this magnetization is feasible within current experimental capabilities, such as employing single-spin microscopy (NV center microscopy) [45] or SQUID magnetometry [46].

In a superconductor-magnet hybrid structure, exchange coupling the superconductor to an adjacent magnet, the supercurrent-induced magnetization can exert the so-called *reactive* torque [47, 48] on the magnet, $\boldsymbol{\tau}_r \sim \boldsymbol{M}(\boldsymbol{q}) \times \boldsymbol{n}$ (even under time-reversal), where $\boldsymbol{n}$ is the magnetization. Reciprocally, the exchange interaction can modify the supercurrent near the interface [49]. Note that in addition to the reactive torque, a current carrying normal metal with SOC (broken inversion symmetry) could in general also exert a *dissipative* torque on the adjacent magnet, $\boldsymbol{\tau}_d \sim \boldsymbol{n} \times \boldsymbol{M}(\boldsymbol{q}) \times \boldsymbol{n}$ (odd under time-reversal). However, the dissipative torque is absent in the superconductor-magnet hybrid structure [50].

In Ref. [51], a spintronic Josephson phase qubit based on spin superfluidity and spin Hall phenomena is proposed in a metal-magnet hybrid structure. The basic idea is that the qubit state can be manipulated by injecting spin current (torque), engendered from an electric current flow in the normal metal with SOC [52]. Motivated by eliminating the Joule heating, a natural generalization of the proposal in Ref. [51] would be to replace the metal with a superconductor. The supercurrent can be used for magnetic qubit manipulations and readout.

In our treatment, we are projecting physical quantities onto a single band, and in doing so, we are neglecting interband coherent effects linked to the quantum metric of the Bloch wave function, discussed in previous works [11, 12, 25–27]. Consequently, without considering these interband effects, under a uniform supercurrent superconducting pair potential remains approximately unchanged and the quasiparticle energies experience a Doppler shift. However, incorporating interband effects introduces an anomalous term for superfluid density, particularly prominent in flat or nearly flat band superconductors [53]. Exploring the impact of these geometric effects on supercurrent-induced magnetization using our formalism would be an interesting future step. In particular, investigating supercurrent-induced magnetization in flat-band superconductors could offer an additional means to explore and probe unconventional superconductivity [54].

We close this Letter by noting that while we have studied the supercurrent-induced magnetization in a clean superconductor (where physically the superconducting gap is much larger than the disorder scattering rate), we expect that our results remain qualitatively valid at a low concentration of impurities. Indeed as shown in Ref. [55], the magnetoelectric effect (spin magnetization), although weakened by impurity scattering, is not destroyed in dirty superconductors where the superconducting gap is smaller than the disorder scattering rate.

It is a pleasure to acknowledge discussions with Allan H. MacDonald. This work was supported by the NSF under Grant No. DMR-2049979.

[1] Jacob Linder and Jason W. A. Robinson, "Superconducting spintronics," Nature Physics **11**, 307 (2015).

[2] Victor M. Edelstein, "Magnetoelectric effect in polar superconductors," Phys. Rev. Lett. **75**, 2004–2007 (1995).

[3] Di Xiao, Ming-Che Chang, and Qian Niu, "Berry phase effects on electronic properties," Rev. Mod. Phys. **82**, 1959–2007 (2010).

[4] Luca Chirolli, Maria Teresa Mercaldo, Claudio Guarcello, Francesco Giazotto, and Mario Cuoco, "Colossal orbital edelstein effect in noncentrosymmetric superconductors," Phys. Rev. Lett. **128**, 217703 (2022).

[5] J. M. Lu, O. Zheliuk, I. Leermakers, N. F. Q. Yuan, U. Zeitler, K. T. Law, and J. T. Ye, "Evidence for two-dimensional ising superconductivity in gated mos2," Science **350**, 1353–1357 (2015); Yu Saito, Yasuharu Nakamura, Mohammad Saeed Bahramy, Yoshimitsu Kohama, Jianting Ye, Yuichi Kasahara, Yuji Nakagawa, Masaru Onga, Masashi Tokunaga, Tsutomu Nojima, Youichi Yanase, and Yoshihiro Iwasa, "Superconductivity protected by spin–valley locking in ion-gated mos2," Nature Physics **12**, 144 (2016); Xiaoxiang Xi, Zefang Wang, Weiwei Zhao, Ju-Hyun Park, Kam Tuen Law, Helmuth Berger, László Forró, Jie Shan, and Kin Fai Mak, "Ising pairing in superconducting nbse2 atomic layers," Nature Physics **12**, 139 (2016); Yanpeng Qi, Pavel G. Naumov, Mazhar N. Ali, Catherine R. Rajamathi, Walter Schnelle, Oleg Barkalov, Michael Hanfland, Shu-Chun Wu, Chandra Shekhar, Yan Sun, Vicky Süß, Marcus Schmidt, Ulrich Schwarz, Eckhard Pippel, Peter Werner, Reinald Hillebrand, Tobias Förster, Erik Kampert, Stuart Parkin, R. J. Cava, Claudia Felser, Binghai Yan, and Sergey A. Medvedev, "Superconductivity in weyl semimetal candidate mote2," Nature Communications **7**, 11038 (2016); Ebrahim Sajadi, Tauno Palomaki, Zaiyao Fei, Wenjin Zhao, Philip Bement, Christian Olsen, Silvia Luescher, Xiaodong Xu, Joshua A. Folk, and David H. Cobden, "Gate-induced superconductivity in a monolayer topological insulator," Science **362**, 922–925 (2018); Valla Fatemi, Sanfeng Wu, Yuan Cao, Landry Bretheau, Quinn D. Gibson, Kenji Watanabe, Takashi Taniguchi, Robert J. Cava, and Pablo Jarillo-Herrero, "Electrically tunable low-density superconductivity in a monolayer topological insulator," Science **362**, 926–929 (2018); Wanying Li, Jinqiang Huang, Xiaoxi Li, Siwen Zhao, Jianming Lu, Zheng Vitto Han, and Hanwen Wang, "Recent progresses in two-dimensional ising superconductivity," Materials Today Physics **21**, 100504 (2021); Aleksi Julku, Jami J. Kinnunen, Arturo Camacho-Guardian, and Georg M. Bruun, "Light-induced topological superconductivity in transition metal dichalcogenide monolayers," Phys. Rev. B **106**, 134510 (2022).

[6] Wen-Yu He, David Goldhaber-Gordon, and K. T. Law, "Giant orbital magnetoelectric effect and current-induced magnetization switching in twisted bilayer

graphene," Nature Communications **11**, 1650 (2020); Si-Yu Li, Yu Zhang, Ya-Ning Ren, Jianpeng Liu, Xi Dai, and Lin He, "Experimental evidence for orbital magnetic moments generated by moiré-scale current loops in twisted bilayer graphene," Phys. Rev. B **102**, 121406 (2020).

[7] C. L. Tschirhart, M. Serlin, H. Polshyn, A. Shragai, Z. Xia, J. Zhu, Y. Zhang, K. Watanabe, T. Taniguchi, M. E. Huber, and A. F. Young, "Imaging orbital ferromagnetism in a moiré chern insulator," Science **372**, 1323–1327 (2021).

[8] Wen-Yu He and K. T. Law, "Superconducting orbital magnetoelectric effect and its evolution across the superconductor-normal metal phase transition," Phys. Rev. Res. **3**, L032012 (2021).

[9] Sasikanth Manipatruni, Dmitri E. Nikonov, Chia-Ching Lin, Tanay A. Gosavi, Huichu Liu, Bhagwati Prasad, Yen-Lin Huang, Everton Bonturim, Ramamoorthy Ramesh, and Ian A. oung, "Scalable energy-efficient magnetoelectric spin–orbit logic," Nature **565**, 35 (2019); Debanjan Polley, Akshay Pattabi, Jyotirmoy Chatterjee, Sucheta Mondal, Kaushalya Jhuria, Hanuman Singh, Jon Gorchon, and Jeffrey Bokor, "Progress toward picosecond on-chip magnetic memory," Applied Physics Letters **120**, 140501 (2022).

[10] B. S. Chandrasekhar and D. Einzel, "The superconducting penetration depth from the semiclassical model," Annalen der Physik **505**, 535–546 (1993).

[11] Long Liang, Sebastiano Peotta, Ari Harju, and Päivi Törmä, "Wave-packet dynamics of bogoliubov quasiparticles: Quantum metric effects," Phys. Rev. B **96**, 064511 (2017).

[12] Akito Daido, Taisei Kitamura, and Youichi Yanase, "Quantum geometry encoded to pair potentials," (2023), https://doi.org/10.48550/arXiv.2310.15558.

[13] T. M. Klapwijk, "Proximity effect from an andreev perspective," Journal of Superconductivity **17**, 593 (2015).

[14] Alessandro Romito, Jason Alicea, Gil Refael, and Felix von Oppen, "Manipulating majorana fermions using supercurrents," Phys. Rev. B **85**, 020502 (2012).

[15] Jason Alicea, Yuval Oreg, Gil Refael, Felix von Oppen, and Matthew P. A. Fisher, "Non-abelian statistics and topological quantum information processing in 1d wire networks," Nature Physics **7**, 412 (2011).

[16] Jian Li, Titus Neupert, B. Andrei Bernevig, F von Oppen, and Ali Yazdani, "Manipulating majorana zero modes on atomic rings with an external magnetic field," Nature Communications **7**, 10395 (2016); Mircea Trif and Pascal Simon, "Braiding of majorana fermions in a cavity," Phys. Rev. Lett. **122**, 236803 (2019); John P. T. Stenger, Nicholas T. Bronn, Daniel J. Egger, and David Pekker, "Simulating the dynamics of braiding of majorana zero modes using an ibm quantum computer," Phys. Rev. Res. **3**, 033171 (2021); Bradraj Pandey, Nitin Kaushal, Gonzalo Alvarez, and Elbio Dagotto, "Majorana zero modes in y-shape interacting kitaev wires," npj Quantum Materials **8**, 51 (2023); Juan Daniel Torres Luna, Sathish R. Kuppuswamy, and Anton R. Akhmerov, "Design of a Majorana trijunction," SciPost Phys. **16**, 044 (2024).

[17] C. W. J. Beenakker, "Search for non-Abelian Majorana braiding statistics in superconductors," SciPost Phys. Lect. Notes , 15 (2020).

[18] Wen-Yu He and K. T. Law, "Magnetoelectric effects in gyrotropic superconductors," Phys. Rev. Res. **2**, 012073 (2020).

[19] Shudan Zhong, Joel E. Moore, and Ivo Souza, "Gyrotropic magnetic effect and the magnetic moment on the fermi surface," Phys. Rev. Lett. **116**, 077201 (2016).

[20] Aline Ramires, Daniel F. Agterberg, and Manfred Sigrist, "Tailoring T_c by symmetry principles: The concept of superconducting fitness," Phys. Rev. B **98**, 024501 (2018).

[21] K. V. Samokhin, E. S. Zijlstra, and S. K. Bose, "cept$_3$Si : an unconventional superconductor without inversion center," Phys. Rev. B **69**, 094514 (2004).

[22] Mark H. Fischer, Manfred Sigrist, and Daniel F. Agterberg, "Superconductivity without inversion and time-reversal symmetries," Phys. Rev. Lett. **121**, 157003 (2018).

[23] Mark H Fischer, "Gap symmetry and stability analysis in the multi-orbital fe-based superconductors," New Journal of Physics **15**, 073006 (2013).

[24] Aline Ramires and Manfred Sigrist, "Identifying detrimental effects for multiorbital superconductivity: Application to sr$_2$ruo$_4$," Phys. Rev. B **94**, 104501 (2016).

[25] Zhi Wang, Liang Dong, Cong Xiao, and Qian Niu, "Berry curvature effects on quasiparticle dynamics in superconductors," Phys. Rev. Lett. **126**, 187001 (2021).

[26] Päivi Törmä, "Essay: Where can quantum geometry lead us?" Phys. Rev. Lett. **131**, 240001 (2023).

[27] Long Liang, Tuomas I. Vanhala, Sebastiano Peotta, Topi Siro, Ari Harju, and Päivi Törmä, "Band geometry, berry curvature, and superfluid weight," Phys. Rev. B **95**, 024515 (2017).

[28] In the Supplementary Material, we provide a derivation of Eq. (2).

[29] Grigory Volovik, "Superconductivity with lines of gap nodes: density of states in the vortex," Soviet Journal of Experimental and Theoretical Physics Letters **58** (1993).

[30] Michael Tinkham, *Introduction to superconductivity* (Courier Corporation, 2004).

[31] P.G. De Gennes, *Superconductivity Of Metals And Alloys (1st ed.)* (CRC Press, 1999).

[32] Ming-Che Chang and Qian Niu, "Berry phase, hyperorbits, and the hofstadter spectrum: Semiclassical dynamics in magnetic bloch bands," Phys. Rev. B **53**, 7010–7023 (1996).

[33] Jing Ma and D. A. Pesin, "Chiral magnetic effect and natural optical activity in metals with or without weyl points," Phys. Rev. B **92**, 235205 (2015).

[34] In Ref. [8], it is assumed that the pairing gap is significantly smaller than the band splitting caused by inversion symmetry breaking. Consequently, certain expressions are derived using the approximation $E_\nu \approx \xi_\nu$ (where the pairing gap is considered negligible), resulting in the appearance of $f(\xi_\nu)$ instead of n_ν.

[35] A. A. Burkov and Leon Balents, "Weyl semimetal in a topological insulator multilayer," Phys. Rev. Lett. **107**, 127205 (2011).

[36] Shun-Qing Shen, *Topological Insulators* (Springer Berlin, Heidelberg, 2013).

[37] Sergio Leiva-Montecinos, Jürgen Henk, Ingrid Mertig, and Annika Johansson, "Spin and orbital edelstein effect in a bilayer system with rashba interaction," Phys. Rev. Res. **5**, 043294 (2023).

[38] Ralph C. Dougherty and J. Daniel Kimel, "Temperature dependence of the superconductor energy gap." (2012),

https://doi.org/10.48550/arXiv.1212.0423.

[39] In the present 2D system, the Hamiltonian does not contain out-of-plane momentum p_z. As a result, to evaluate derivative with respect to p_z in Eq. (4) we use [32]

$$\langle u_{\nu',\boldsymbol{p}}|\nabla_{\boldsymbol{p}}u_{\nu,\boldsymbol{p}}\rangle = \frac{\langle u_{\nu',\boldsymbol{p}}|\nabla_{\boldsymbol{p}}H_0|u_{\nu,\boldsymbol{p}}\rangle}{\xi_{\nu'}-\xi_{\nu}},$$

for the interband Berry connection (i.e., $\nu \neq \nu'$) with

$$\langle u_{\nu,\boldsymbol{p}}|\frac{\partial H_0}{\partial p_z}|u_{\nu',\boldsymbol{p}}\rangle \to -\frac{i}{\hbar}\langle u_{\nu,\boldsymbol{p}}|[\hat{\mathfrak{z}},H_0]|u_{\nu',\boldsymbol{p}}\rangle,$$

where $\hat{\mathfrak{z}} = \mathrm{diag}(\frac{t}{2},-\frac{t}{2})\otimes\sigma_0$ can be considered as the out-of-plane component of the position operator with t being the distance between the layers [37, 56]. In particular, after some straightforward algebra, we obtain

$$m_{\nu y}(\boldsymbol{p}) = e\mathrm{Re}\Big[\langle u_{\nu,\boldsymbol{p}}|\hat{\mathfrak{z}}|u_{\nu,\boldsymbol{p}}\rangle\langle u_{\nu,\boldsymbol{p}}|v_x|u_{\nu,\boldsymbol{p}}\rangle - \langle u_{\nu,\boldsymbol{p}}|\hat{\mathfrak{z}}v_x|u_{\nu,\boldsymbol{p}}\rangle\Big],$$

where $v_x = \frac{\partial H_0}{\partial p_x}$.

[40] Yu A Bychkov and E I Rashba, "Oscillatory effects and the magnetic susceptibility of carriers in inversion layers," Journal of Physics C: Solid State Physics **17**, 6039 (1984).

[41] Yuval Oreg, Gil Refael, and Felix von Oppen, "Helical liquids and majorana bound states in quantum wires," Phys. Rev. Lett. **105**, 177002 (2010).

[42] Kazuaki Takasan, Shuntaro Sumita, and Youichi Yanase, "Supercurrent-induced topological phase transitions," Phys. Rev. B **106**, 014508 (2022).

[43] S. M. Albrecht, A. P. Higginbotham, M. Madsen, F. Kuemmeth, T. S. Jespersen, J. Nygård, P. Krogstrup, and C. M. Marcus, "Exponential protection of zero modes in majorana islands," Nature **531**, 206 (2016); Georg W. Winkler, Dániel Varjas, Rafal Skolasinski, Alexey A. Soluyanov, Matthias Troyer, and Michael Wimmer, "Orbital contributions to the electron g factor in semiconductor nanowires," Phys. Rev. Lett. **119**, 037701 (2017).

[44] The strngth of SOC in Bi/Ag bilyers is comparable to this value [**?** **?**]. Here, we provide estimates for spin and orbital magnetizations in the bilayer Rashba system with the following parameters: $\lambda = 2.5$ meV, $\Delta_0 = 5$ meV, $\mu = 0.3$ eV, $T = 0.1T_c$, $t = 2$ Å, $g = 2$, $m_e = 0.3m_0$, where m_0 is the electron bare mass. For the Cooper pair momentum q, we consider the inverse of the superconducting coherence length ξ, $\hbar/\xi$, as an upper limit.

[45] L. Thiel, Z. Wang, M. A. Tschudin, D. Rohner, I. Gutiérrez-Lezama, N. Ubrig, M. Gibertini, E. Giannini, A. F. Morpurgo, and P. Maletinsky, "Probing magnetism in 2d materials at the nanoscale with single-spin microscopy," Science **364**, 973–976 (2019).

[46] C. L. Tschirhart, M. Serlin, H. Polshyn, A. Shragai, Z. Xia, J. Zhu, Y. Zhang, K. Watanabe, T. Taniguchi, M. E. Huber, and A. F. Young, "Imaging orbital ferromagnetism in a moiré chern insulator," Science **372**, 1323–1327 (2021).

[47] Yaroslav Tserkovnyak and Scott A. Bender, "Spin hall phenomenology of magnetic dynamics," Phys. Rev. B **90**, 014428 (2014).

[48] F. Sebastian Bergeret and Ilya V. Tokatly, "Manifestation of extrinsic spin hall effect in superconducting structures: Nondissipative magnetoelectric effects," Phys. Rev. B **94**, 180502 (2016).

[49] S. Mironov and A. Buzdin, "Spontaneous currents in superconducting systems with strong spin-orbit coupling," Phys. Rev. Lett. **118**, 077001 (2017).

[50] The dissipative torque is also absent in a current-carrying 2D massless Dirac system [47], which arises on the surfaces of strong 3D topological insulators [57].

[51] So Takei, Yaroslav Tserkovnyak, and Masoud Mohseni, "Spin superfluid josephson quantum devices," Phys. Rev. B **95**, 144402 (2017).

[52] A. Manchon and S. Zhang, "Theory of nonequilibrium intrinsic spin torque in a single nanomagnet," Phys. Rev. B **78**, 212405 (2008); "Theory of spin torque due to spin-orbit coupling," Phys. Rev. B **79**, 094422 (2009).

[53] Kukka-Emilia Huhtinen, Jonah Herzog-Arbeitman, Aaron Chew, Bogdan A. Bernevig, and Päivi Törmä, "Revisiting flat band superconductivity: Dependence on minimal quantum metric and band touchings," Phys. Rev. B **106**, 014518 (2022).

[54] P. Törmä, S. Peotta, and B. A. Bernevig, "Superconductivity, superfluidity and quantum geometry in twisted multilayer systems," Nature Reviews Physics **4**, 528 (2022).

[55] Victor M. Edelstein, "Magnetoelectric effect in dirty superconductors with broken mirror symmetry," Phys. Rev. B **72**, 172501 (2005).

[56] Daisuke Hara, M. S. Bahramy, and Shuichi Murakami, "Current-induced orbital magnetization in systems without inversion symmetry," Phys. Rev. B **102**, 184404 (2020).

[57] M. Z. Hasan and C. L. Kane, "Colloquium: Topological insulators," Rev. Mod. Phys. **82**, 3045–3067 (2010).